

# Ultrashort x-ray pulse generation by electron beam slicing in storage rings

A. He, F. Willeke, and L. H. Yu

Photon Sciences Directorate, Brookhaven National Laboratory, Upton, New York 11973, USA

(Received 20 August 2013; published 4 April 2014)

We propose a new method to generate ultrashort x-ray pulses using focused short low energy ( $\sim 20$  MeV) electron bunches to create short slices of electrons from the circulating electron bunches in a synchrotron radiation storage ring. When a low energy electron bunch crosses from the top of a high energy storage ring electron bunch, its Coulomb force will kick a short slice from the core of the storage ring electron bunch. The separated slices, when passing through an undulator, will radiate ultrashort x-ray pulses at about 160 fs. We discuss the advantages, challenges, and provide data which confirm the feasibility of this new method.

DOI: [10.1103/PhysRevSTAB.17.040701](https://doi.org/10.1103/PhysRevSTAB.17.040701)

PACS numbers: 52.59.Px, 29.20.dk, 41.60.Cr

## I. BASIC PRINCIPLES AND PARAMETERS

The community interested in science using sub-picosecond x-ray pulses is growing rapidly. Laser slicing is one of the approaches to generate ultrashort x-ray pulse [1–6]. Typically, for laser slicing the x-ray pulses are of the order of 100 fs with repetition rate of order of 1 kHz and the number of photons per 0.1% bandwidth per pulse is of the order of 1000. To generate ultrashort x-ray pulses with many orders of magnitude higher repetition rate, another method is proposed by Zholents [7,8] using a crab cavity which provides pulse length of order of a picosecond. It provides a continuous stream of x-ray pulses [9] with a much higher average flux. A new source of ultrashort x-ray pulses is x-ray free electron laser, with the pulse energy many orders of magnitude higher than storage ring and pulse width of 100 fs or less [10]. However, compared with the storage ring sources, the fluctuation of the intensity and wavelength from a SASE FEL is large, and the repetition rate is low. For example, the repetition rate of LCLS SASE FEL is 120 Hz [11]. Hence, even though the single pulse energy is much lower than the SASE FEL pulse, the high repetition rate and high pulse to pulse stability of storage ring sources continue to attract a wide range of user interests.

In this paper we propose a different approach to generate ultrashort x-ray pulses of the order of 100 fs pulse length by electron beam slicing [12]. As shown in Fig. 1, when a short electron bunch from a low energy linac (for example, 20 MeV, 200 pC, 150 fs) passes 35  $\mu\text{m}$  above a storage ring bunch (30 ps) at a right angle, it kicks a short slice ( $\sim 160$  fs) of electron bunch vertically. The radiation from the short slice is separated from the core bunch. We find the

following advantages of this method when it is compared with other schemes respectively: (i) when compared with crab cavity method, it needs much smaller space in storage ring for interaction, and its radiation pulse length ( $\sim 160$  fs) is much shorter. (ii) When compared with laser slicing method, its flux per pulse may be increased significantly, by a factor of from 6 to 10 (the flux is discussed in Sec. VA), and the repetition rate can be much higher while the pulse length is comparable. (iii) When compared with LCLS SASE x-ray free electron laser, its repetition rate can be  $10^3$ – $10^4$  orders of magnitude higher, and it is much more stable, even though the single shot pulse energy is many orders of magnitude lower.

Thus we expect the new method may provide a complementary approach to other ultrashort x-ray pulse sources.

## II. DERIVATION OF THE KICK ANGLE

### A. Angular kick function

We explored the new method by calculating the angular kick received by a high energy electron (labeled as bunch 1), generated by a point charge in the low energy

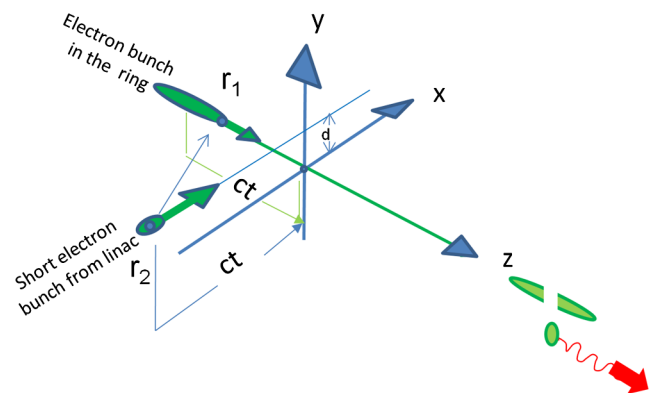


FIG. 1. Illustration of electron beam slicing.

Published by the American Physical Society under the terms of the [Creative Commons Attribution 3.0 License](https://creativecommons.org/licenses/by/3.0/). Further distribution of this work must maintain attribution to the author(s) and the published article's title, journal citation, and DOI.

linac electron bunch (labeled as bunch 2) and integrated over the 3D electron distribution of the low energy bunch.

The electric field at position  $\vec{r}_1$  contributed by the electron 2 at position  $\vec{r}_2$  can be expressed by [13]

$$\vec{E} = \frac{e}{4\pi\epsilon_0} \frac{\gamma_2}{S^3} \vec{r}, \quad (1)$$

where  $\epsilon_0$  is the permittivity of free space,  $S = \sqrt{\gamma_2^2 x^2 + y^2 + z^2}$ ,  $\vec{r} = \vec{r}_1 - \vec{r}_2$ . The corresponding magnetic field can be calculated by  $c\vec{B} = \vec{\beta}_2 \times \vec{E}$ . Using  $\vec{F} = e\vec{E} + e\vec{v}_1 \times \vec{B}$ , assuming that when  $t = 0$  electron 1 locates at position  $(x_1, y_1, z_1)$  and electron 2 locates at position  $(x_2, y_2 + d, z_2)$ , where  $d$  is the vertical distance between the storage ring beam line and the low energy beam line, and assuming each low energy particle's point charge is  $q_2$ , the kick force on electron 1 in the vertical direction can be expressed as

$$F_y = -\frac{eq_2}{4\pi\epsilon_0} \frac{\gamma_2}{S^3} (d + y_2 - y_1). \quad (2)$$

The relation between the kick force and the kick angle can be expressed as

$$F_y = \gamma_1 mc \frac{d\theta_y}{dt} = \frac{E_1}{c} \frac{d\theta_y}{dt}, \quad (3)$$

where we use  $\frac{dy}{dt} \approx \frac{cdy}{dz_1} = c\theta_y$  due to  $v_{z_1} \approx c$ ,  $E_1$  is the energy of the storage ring electron 1. The angular kick  $\Delta\theta_y$  generated by a point charge in the low energy bunch 2 can be obtained by integrating  $d\theta_y = (cF_y/E_1)dt$  over the crossing time:

$$\begin{aligned} \Delta\theta_y &= \frac{eq_2\gamma_2 c}{4\pi\epsilon_0 E_1} \int_{-\infty}^{+\infty} \frac{dt}{S^3} (d + y_2 - y_1) \\ &= \frac{eq_2 Z_0 c}{2\pi E_1} \cdot \frac{\gamma_2}{\sqrt{\gamma_2^2 + 1}} \cdot \frac{d + y_2 - y_1}{a^2}, \end{aligned} \quad (4)$$

where  $Z_0 = \frac{1}{\epsilon_0 c} = 377 \Omega$  and

$$a^2 = \frac{\gamma_2^2}{\gamma_2^2 + 1} \times [(x_2 - x_1) + (z_2 - z_1)]^2 + (d + y_2 - y_1)^2.$$

In Eq. (4), we removed a minus sign for the  $\Delta\theta_y$  which is due to the minus sign of Eq. (2). This means we define  $\Delta\theta_y$  as positive if the electron is kicked downward in Fig. 1.

We assume the low energy bunch 2 has a Gaussian distribution in the  $x, y, z$  direction and the rms bunch size is  $\sigma_x, \sigma_y, \sigma_z$ . Integrating  $\Delta\theta_y$  over the whole low energy bunch 2, we obtain the angular kick as a function of the 3D position of an electron in the storage ring bunch:

$$\Delta\theta_y = \frac{eq_2 Z_0 c}{2\pi E_1} \frac{\gamma_2}{\sqrt{\gamma_2^2 + 1}} \frac{1}{\sqrt{2}\sigma_y} f(\rho, \bar{u}_1, \bar{y}_1), \quad (5)$$

where  $f$  gives the profile as a function of the position of the high energy electron:

$$\begin{aligned} f(\rho, \bar{u}_1, \bar{y}_1) &= \int_0^\infty \text{Re}[W(\bar{u}_1 + iy)][e^{-(\rho y - \bar{y}_1)^2} - e^{-(\rho y + \bar{y}_1)^2}] dy, \end{aligned} \quad (6)$$

with

$$\begin{aligned} \rho &= \sqrt{\frac{\gamma_2^2}{\gamma_2^2 + 1} \cdot \frac{\sigma_x^2 + \sigma_z^2}{\sigma_y^2}}, \\ \bar{y}_1 &= \frac{d - y_1}{\sqrt{2}\sigma_y}, \\ \bar{u}_1 &= \frac{x_1 + z_1}{\sqrt{2(\sigma_x^2 + \sigma_z^2)}}, \end{aligned} \quad (7)$$

$d$  is the vertical distance between the centers of the low energy beam and the high energy beam.  $x_1, y_1, z_1$  are the coordinates of the high energy electron,  $\sigma_x, \sigma_y, \sigma_z$  are the rms beam size of the low energy bunch.  $q_2$  is the charge of low energy bunch,  $\gamma_2$  is its dimensionless energy,  $Z_0 = 377 \Omega$  is the vacuum impedance.  $W$  is the error function:  $W(u) = e^{-u^2} \text{erfc}(-iu)$ .

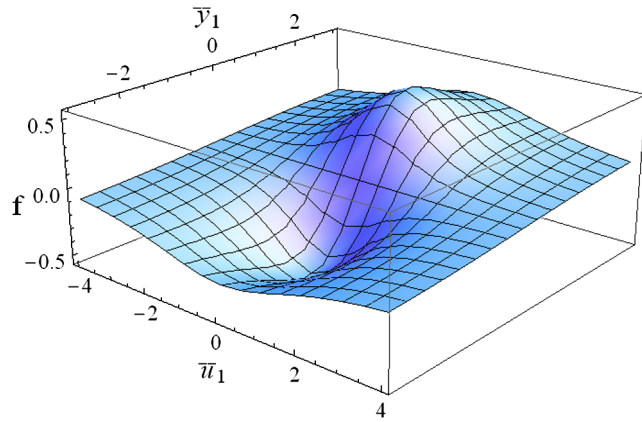
The angular kicks in the horizontal and the longitudinal direction, received by the high energy bunch, are discussed in [14]. The analysis shows that the horizontal angular kick is much smaller than the angular spread of the high energy beam, while the energy modulation generated by the longitudinal kick is negligible compared with the energy spread of the high energy bunch. To be brief, we will not go into details of these here.

## B. Analysis of the kick angle and kick profile

As a numerical example using NSLS-II parameters [15], we assume the kick point is at a position in the ring where  $\beta_x = 3.8$  m,  $\beta_y = 25$  m. If the vertical emittance is 10 pm, the rms beam divergence is  $\sigma'_y = 0.6 \mu\text{rad}$ . To separate the slice from the core we need the angular kick more than 5 times larger, i.e.,  $3 \mu\text{rad}$ . We assume the 20 MeV electron bunch with charge of  $q_2 = 200$  pC is focused to the size of  $\sigma_x = \sigma_y = 35 \mu\text{m}$ , and compressed to  $\sigma_z = 35 \mu\text{m}$ , i.e., bunch length of about 120 fs. We have  $Z_0 = 377 \Omega$ ,  $E_1 = 3$  GeV,  $E_2 = 20$  MeV, hence we find the nominal kick angle as

$$\begin{aligned} \Delta\theta_0 &= \frac{eq_2 Z_0 c}{2\pi E_1} \frac{\gamma_2}{\sqrt{\gamma_2^2 + 1}} \frac{1}{\sqrt{2}\sigma_y} \\ &= \frac{e \times 200 \text{ pC} \times 377 \Omega}{2\pi \times 3 \text{ GeV}} \times \frac{3 \times 10^8 \text{ m/s}}{50 \mu\text{m}} \\ &= 24 \mu\text{rad}. \end{aligned}$$

The profile parameter

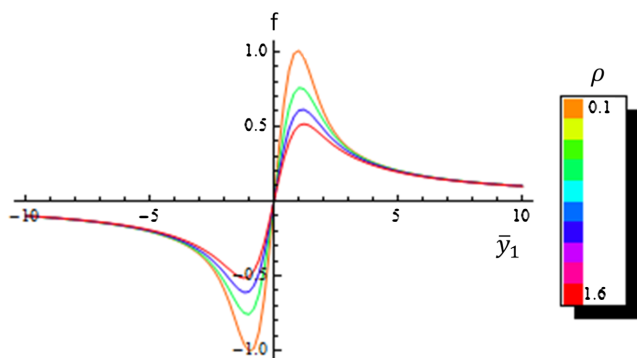
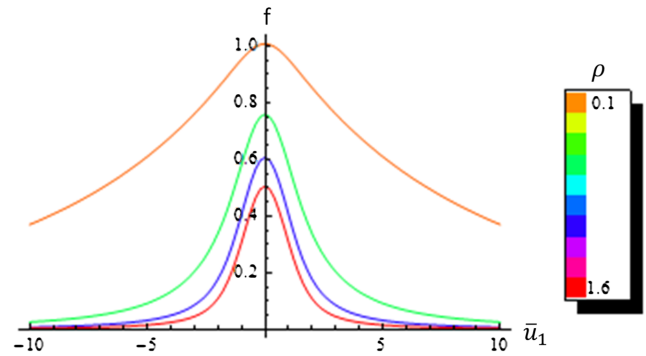

 FIG. 2. Profile function  $f$ .

$$\rho = \sqrt{\frac{\gamma_2^2}{\gamma_2^2 + 1} \cdot \frac{\sigma_x^2 + \sigma_z^2}{\sigma_y^2}} = 1.4.$$

We choose the distance between the storage ring beam line and the low energy beam line as  $d = \sqrt{2}\sigma_y = 50 \mu\text{m}$ , which we find to give maximum kick. Assume  $x_1 = y_1 = z_1 = 0$ , i.e., when the electron in the storage ring bunch arrives at the origin of the coordinate system, the center of low energy bunch just arrives at the position on top of the origin by vertical distance  $d = 50 \mu\text{m}$ , then we have  $\bar{y}_1 = 1$ ,  $\bar{u}_1 = 0$ , and we find  $f = 0.54$ . The kick angle is then given by  $\theta = \theta_0 f = 24 \mu\text{rad} \times 0.54 = 13 \mu\text{rad}$ , much larger than the required  $3 \mu\text{rad}$  for the separation from the core.

To understand the profile of the angular kick, we plot the function  $f$  in Fig. 2 for the case of  $\rho = 1.4$ . A set of plots of  $f$  as a function of  $\bar{y}_1$  at  $\bar{u}_1 = 0$  for different  $\rho$  is shown in Fig. 3. The maximum is always approximately at  $\bar{y}_1 = 1$ .

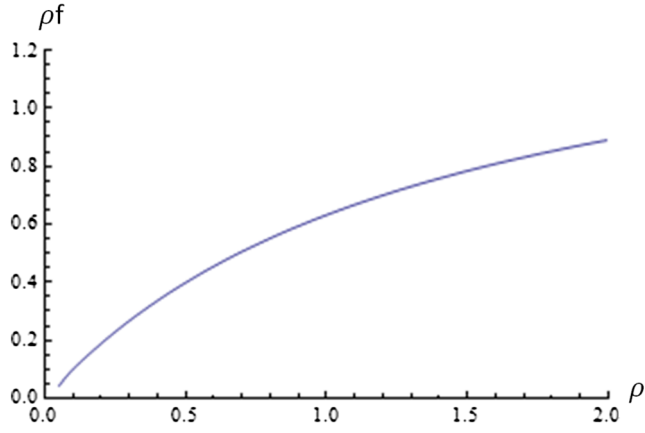
We also plot the profile of  $f$  as a function of  $\bar{u}_1$  for  $\bar{y}_1 = 1$  in Fig. 4 for different  $\rho$ . The width in  $\bar{u}_1$  of the profile  $f$  at  $\bar{y}_1 = 1$  can be used to estimate the width of the slice. From Eq. (7), we have


 FIG. 3. Profile on axis  $\bar{u}_1 = 0$ . The maximum  $f$  locates at  $\bar{y}_1 = 1$ .

 FIG. 4. Profile on axis  $\bar{y}_1 = 1$ . Show that decreasing  $\rho$  will increase the pulse width. If we need  $\rho \sim 1$  or  $\rho > 1$ , we need small  $\sigma_y$ .

$$z_1 = \sqrt{2(\sigma_x^2 + \sigma_z^2)}\bar{u}_1 - x_1. \quad (8)$$

This equation shows the slice width is affected by two independent terms: one term, being proportional to  $\bar{u}_1$ , due to the vertical kick from the linac bunch and the other term, being proportional to  $x_1$ , due to the horizontal crossing time of the low energy bunch when it passes across the high energy bunch from top. These terms add in quadrature to provide the slice width. To estimate the slice width, we assume the horizontal distribution of the storage ring bunch and the 3D distribution of the slice bunch are Gaussian, and we also approximate the profile of  $\bar{u}_1$  as Gaussian. For the above example, at the kick point with  $\beta_x = 3.8 \text{ m}$  and  $\varepsilon_x = 1 \text{ nm}$ , the horizontal FWHM of the storage ring bunch is about  $145 \mu\text{m}$  and at  $\rho = 1.4$  the FWHM of  $\bar{u}_1$  is 2.5. Then the estimated FWHM of the slice bunch is about  $227 \mu\text{m}$  which corresponds to 760 fs. As an estimate, we use an aperture to select x rays from those electrons in the slice whose kick angle is larger than half of the maximum kick angle, then the peak to peak pulse width of the slice is 760 fs. Thus the estimated rms value of slice width should be estimated roughly as one-fourth of this peak to peak value, i.e., 190 fs. (This can only serve as an order of magnitude estimate. The simulation result is given in Sec. VA.) We can see the contribution of the horizontal crossing time dominates the pulse width. But, as we will discuss in more detail later in Sec. VA, we find that when the low energy bunch crosses the high energy bunch with an angle of  $45^\circ$  rather than  $90^\circ$ , this problem of horizontal crossing time can be overcome. Then, again, the width of  $\bar{u}_1$  becomes important, and we can reach the slice length of the order of 150 fs.

To see how the width of the slice depends on  $\rho$ , we examine Fig. 4 for different  $\rho$ . This plot shows that to reduce the width we need to increase  $\rho$  to more than 1. But Fig. 4 also indicates that when  $\rho$  increases the maximum value of  $f$  decreases. However, we notice that the nominal kick angle  $\theta_0$  is inversely proportional to  $\sigma_y$ , since  $\rho$  is also inversely proportional to  $\sigma_y$ , the kick angle is proportional

FIG. 5.  $\rho f$  increases as a function of  $\rho$ .

to  $\rho f$ . In Fig. 5, we plot  $\rho f$  as a function of  $\rho$ , and we find that when  $\rho$  increases,  $\rho f$  increases. Hence from both the point of view of reducing pulse width and increasing the kick angle, we favor the increase of  $\rho$ . As a result, even though it is important to have  $\sigma_x, \sigma_y, \sigma_z$  small, it is even more important to have  $\sigma_y$  smaller to reduce the pulse length and increase the kick angle. Thus it is favorable to have a pancake shape for the low energy bunch at the focal point with thin dimension in the vertical direction. This is easy to understand, because the maximum kick angle is at the edge of the low energy bunch, when  $\sigma_y$  is smaller, the position of maximum kick is closer to the center of the low energy bunch, and because the width of the kick angle profile decreases with increased  $\rho$ , hence decreased  $\sigma_y$ .

### C. Reaction from high energy bunch to low energy bunch

We also need to estimate the angular kick received by the electrons in the low energy bunch, caused by the high energy bunch. To calculate the reaction of the high energy bunch to the low energy bunch, we use Eq. (5) and change the notations. Now “2” refers to the high energy bunch and “1” refers to the low energy bunch. Then for the high energy bunch, the axis “+x,” “+y” and “+z” are the longitudinal, vertical and horizontal direction respectively. We use the same beam parameters given in the previous example to give an explanation that the reaction can be ignored.

At the kick point, the related parameters of the high energy bunch are  $\sigma_x = 15 \text{ ps} \times 3 \times 10^8 \text{ m/s} = 4.5 \text{ mm}$ ,  $\sigma_y = \sqrt{25 \text{ m} \times 10^{-11} \text{ m}} = 15.8 \text{ } \mu\text{m}$ ,  $\sigma_z = \sqrt{3.8 \text{ m} \times 10^{-9} \text{ m}} = 61.6 \text{ } \mu\text{m}$ ,  $q_2 = \frac{0.5 \text{ A} \times 2.63 \text{ } \mu\text{s}}{1000} = 1.3 \text{ nC}$  (for beam current of 0.5 A, assume 1000 bunches, with the revolution time of 2.63  $\mu\text{s}$ , we have the bunch charge as 1.3 nC),  $E_1 = 20 \text{ MeV}$ ,  $\gamma_2 = \frac{3 \text{ GeV}}{0.511 \text{ MeV}} = 6000$ . In order to estimate the maximum reaction, we choose crossing angle  $\rho = 90^\circ$ , then

$$\begin{aligned} \theta_y(90^\circ) &= \frac{eq_2 Z_0 c}{2\pi E_1} \frac{\gamma_2}{\sqrt{\gamma_2^2 + 1}} \frac{1}{\sqrt{2}\sigma_y} \times f_y(\rho, \bar{u}_1, \bar{y}_1) \\ &= 0.05 \times f_y(\rho, \bar{u}_1, \bar{y}_1), \end{aligned}$$

where  $f_y(\rho, \bar{u}_1, \bar{y}_1)$  is the profile function. For this storage ring bunch, the profile parameter

$$\rho = \sqrt{\frac{\gamma_2^2}{\gamma_2^2 + 1} \cdot \frac{\sigma_x^2 + \sigma_z^2}{\sigma_y^2}} = 285.$$

We also choose the same kick situation given in the previous example in Sec. II B, then  $\bar{u}_1 = 0$ ,  $\bar{y}_1 = 1$ . Thus the profile function  $f_y(\rho = 284, \bar{u}_1 = 0, \bar{y}_1 = 1) \approx 0.0052$  and the reaction on the low energy bunch is

$$\begin{aligned} \theta_y(90^\circ) &= 0.05 \times f_y(\rho = 285, \bar{u}_1 = 0, \bar{y}_1 = 1) \\ &= 0.05 \times \frac{\sqrt{\pi}}{\rho} \text{erf}(\bar{y}_1) \approx 0.26 \text{ [mrad]}, \end{aligned} \quad (9)$$

where  $\text{erf}(z) = \frac{2}{\sqrt{\pi}} \int_0^z e^{-t^2} dt$  and the detailed derivation is given in Appendix A. We assume the vertical beam size of the low energy bunch is 35  $\mu\text{m}$ . Then during the interaction time, the low energy bunch’s position will be changed about 0.009  $\mu\text{m}$  in the vertical direction which can be ignored when compared with the vertical beam size 35  $\mu\text{m}$ .

### III. BUNCH COMPRESSOR SIMULATION

To minimize cost, the linac bunch energy should be as low as possible. We investigated slicing with a low energy  $\sim 20 \text{ MeV}$ , high charge  $\sim 200 \text{ pC}$  beam. For such low energy and high charge beam, the final focus is in the space charge dominated regime which represents a challenge for the design of an electron gun and magnetic chicane system for the compression. While our result shows that we can achieve our initial goal as given in the above example quite closely, an increase of the energy and the charge of the low energy electron bunch would further reduce the length of the x-ray pulses and increase the angular kick. This analysis provides a reference for the future design of an electron beam slicing system.

We carried out a simulation study to design a system consisting of the LBNL’s VHF gun operating at 186 MHz [16], superconducting rf cavity at 1.3 GHz, several

TABLE I. Performances of the compressor.

Case	Charge [pC]	Energy [MeV]	$\sigma_L^a$ [fs]	$\sigma_H^b$ [ $\mu\text{m}$ ]	$\sigma_V^c$ [ $\mu\text{m}$ ]
1	150	18	130	47	28
2	200	20	148	46	25
3	200	22	128	42	25

<sup>a</sup>The longitudinal rms bunch length of the linac bunch.<sup>b</sup>The horizontal rms beam size of the linac bunch.<sup>c</sup>The vertical rms beam size of the linac bunch.

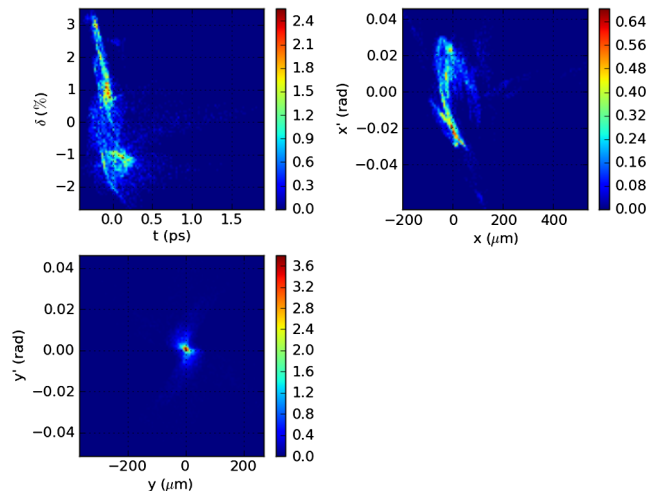


FIG. 6. The histograms of 6D phase space at the final focus point of the compressor. The color bar shows the particle density.

solenoids and a compressor chicane with a matching section. We assume the field gradient is 20 MV/m at the cathode. The simulation code used is IMPACT-T [17]. To check the effect of the coherent synchrotron radiation (CSR), we compared the simulation results with the results when the CSR effect is turned off in IMPACT-T, and also compared with simulation using the code PARMELA which does not take CSR into account [18]. Our comparison shows that the CSR effect is negligible in our case. We carried out a multiobjective optimization procedure using the genetic algorithm [19], allowing the laser pulse length, the laser spot size, the phases and amplitudes of the gun and accelerating cavity, the field strengths of quads and dipoles in the chicane to vary with the two target functions set: the sum of transverse rms beam sizes, and the bunch length respectively. Some optimized results are shown in Table I. For example, at 20 MeV with 200 pC charge and a 8.7 m compressor chicane, the optimization leads to 148 fs rms bunch length at the focal point with 46  $\mu\text{m}$ , and 25  $\mu\text{m}$  for horizontal and vertical rms beam size respectively. Figure 6 shows the histograms of 6D phase space at the final focus point of the compressor with the color bar indicating the particle density. A more detailed description is to be found in [20].

#### IV. PHOTON FLUX AND REPETITION RATE

Before the discussion about the photon flux in the radiator, we need to discuss the separation between the slice bunch and the core bunch. To improve the separation of the synchrotron radiation of the satellite from the core, we would like to maximize this angular deflection at the radiator. This is realized by maximizing the vertical beta function at the crossing point while minimizing the vertical beta function at the radiator and at the same time keeping as close as possible to  $180^\circ$  vertical betatron phase advance between the two points. For the example in Sec. II B, the slice bunch receives a 13  $\mu\text{rad}$  vertical deflection at the

crossing point. If we choose the vertical beta functions  $\beta_{y,\text{kick}} = 25$  m at the crossing point and  $\beta_{y,\text{radiator}} = 1$  m at the radiator, and choose the phase advance  $\Delta\phi = 180^\circ$  between the two points, the kick angle increases from 13 to 65  $\mu\text{rad}$  at the radiator.

If we use a 20 mm period in-vacuum undulator of NSLS-II as the radiator [15], the photon flux for 8 keV x rays is  $10^{15}$  photons/sec/0.1%BW for a beam current 500 mA. With about 1000 bunches, bunch current is 0.5 mA. As an estimate, for a slice of 0.3 ps out of the 30 ps core bunch length (for NSLS-II, rms bunch length is 15 ps [15]) the slice fraction is 0.3 ps/30 ps = 1%. Since revolution time is about 2.6  $\mu\text{s}$ , the single pulse photon flux is  $10^{15} \times 0.3$  ps/30 ps  $\times$  2.6  $\mu\text{s}$ /1000 =  $2.6 \times 10^4$  photons/0.1%BW. If we choose a camshaft current of 3 mA (in the multibunch operation of the storage ring, one or several bunches may be injected with higher charge than other bunches—these bunches are called “camshaft bunches” and the bunch current of a camshaft bunch is called camshaft current), the flux can be increased to  $15.6 \times 10^4$  photons/0.1%BW. When compared with laser slicing, the method by electron beam slicing has more photons per pulse than the laser slicing by a factor of 6–10. The main reason for this is that in laser slicing when the energy modulated electrons pass through the undulator with dispersion, within one optical period there is only a fraction  $\eta$  of electrons [see Eq. (13) of Ref. [1] by Zholents] that fall within the right energy range so their transverse position allows them to be separated from the core electrons. This fraction is about 10%–15%. For electron beam slicing, the electrons within the whole slice kicked out contribute to the radiation, without the additional fraction factor  $\eta$ . Thus we expect about 6–10 times increase of photon flux per pulse by this method.

The emittance increase sets the limitation on the repetition rate. For a single bunch, the emittance increase due to angular kicks is equal to the emittance increase rate times the damping time. One angular kick of  $5\sigma'_y$  with a slice of 300 fs in a 30 ps bunch increases  $\epsilon_y$  by 0.3 ps/30 ps  $\times$   $5^2 \times 1/2\epsilon_y = 12\%\epsilon_y$ . The emittance increase induced by a kick is explained in more detail in Appendix B. With a repetition rate of 100 Hz for a single bunch, and damping time of 10 ms, the emittance increase is  $12\%\epsilon_y \times 100$  Hz  $\times$  10 ms =  $12\%\epsilon_y$ . If we distribute the kicks uniformly over all 1000 bunches, the repetition rate would be 100 kHz. For 100 kHz repetition rate, the photon flux is  $2.6 \times 10^9$  photons/sec/0.1%BW for the example above. For most synchrotron light source users, the requirement on vertical emittance is not very stringent. Thus depending on the tolerance of the vertical emittance increase, the repetition rate limit can be 100 kHz to 1 MHz at the expense of a slightly reduced separation for the same kick.

If after a betatron phase advance of  $\pi$  or a multiple integer of  $\pi$ , another low energy electron bunch, synchronized with and identical to the first one but

precisely time delayed and positioned, will kick the sliced electron bunch back into the separated core bunch, as shown in Fig. 7. This second low energy electron bunch allows the storage ring high energy electron bunch slice

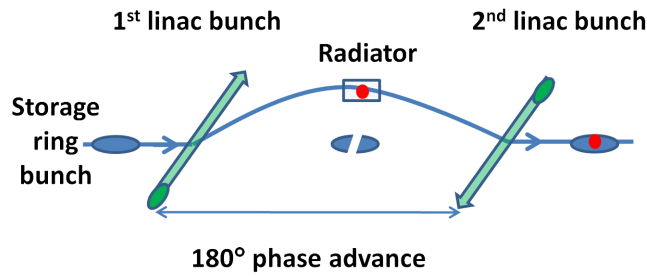


FIG. 7. Two linac bunches form a local bump for the kicked electrons in the storage ring.

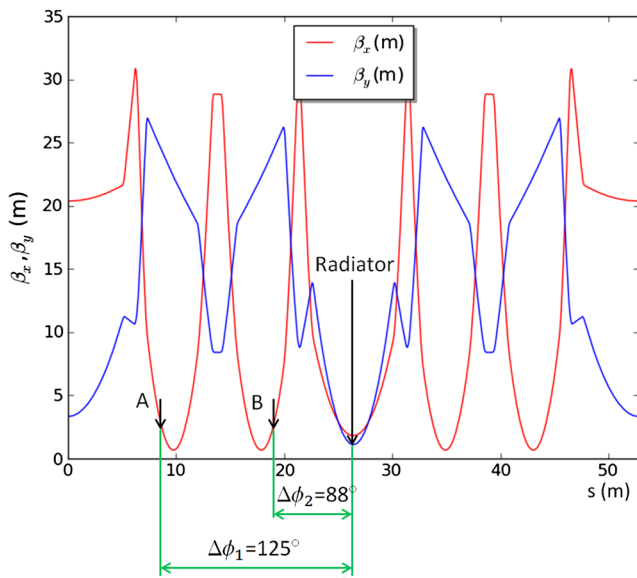


FIG. 8. NSLS-II lattice.

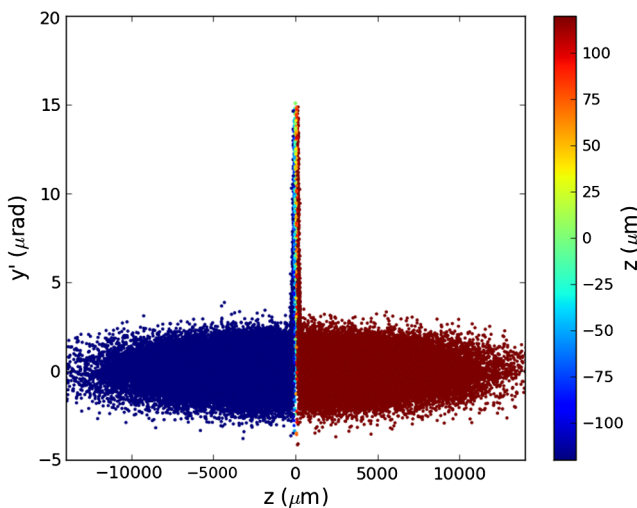


FIG. 9. Phase space for  $y'$  versus  $z$  at the crossing point at 8.3 m right after the kick.

to pass through a local bump and recover its distribution after the radiation, thus minimizing the perturbation to the storage ring so that it is possible to increase the repetition rate significantly. If the time jitter is 10% of the pulse width [21], the repetition rate will increase to 1–10 MHz. These options present a number of challenges yet to be studied.

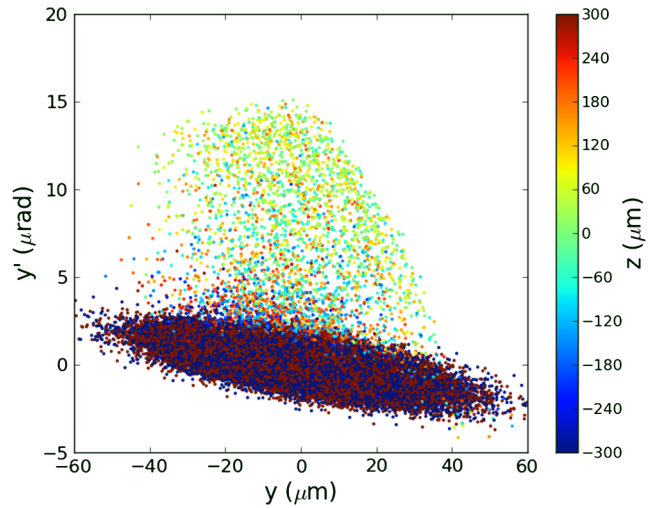


FIG. 10. Phase space for  $y$  versus  $y'$  at the crossing point at 8.3 m right after the kick.

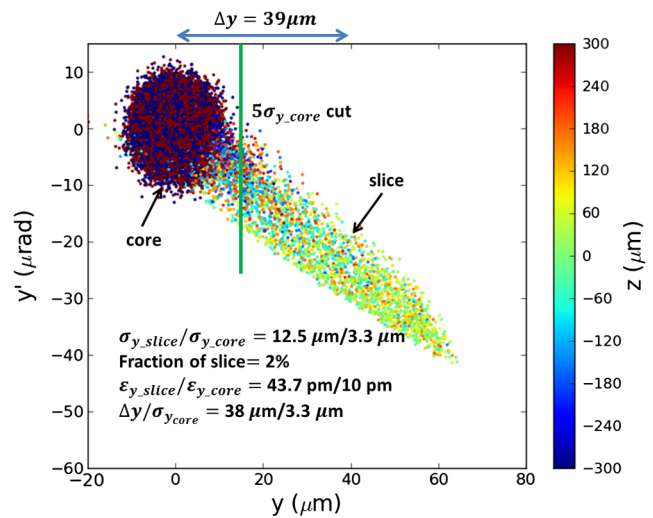


FIG. 11. Phase space for  $y$  versus  $y'$  right at the radiator at 26 m.

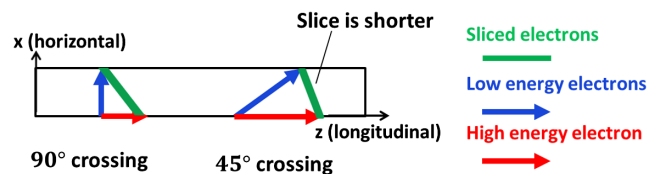


FIG. 12. Illustration of using 45° crossing to reduce crossing time and reduce the slice pulse length.

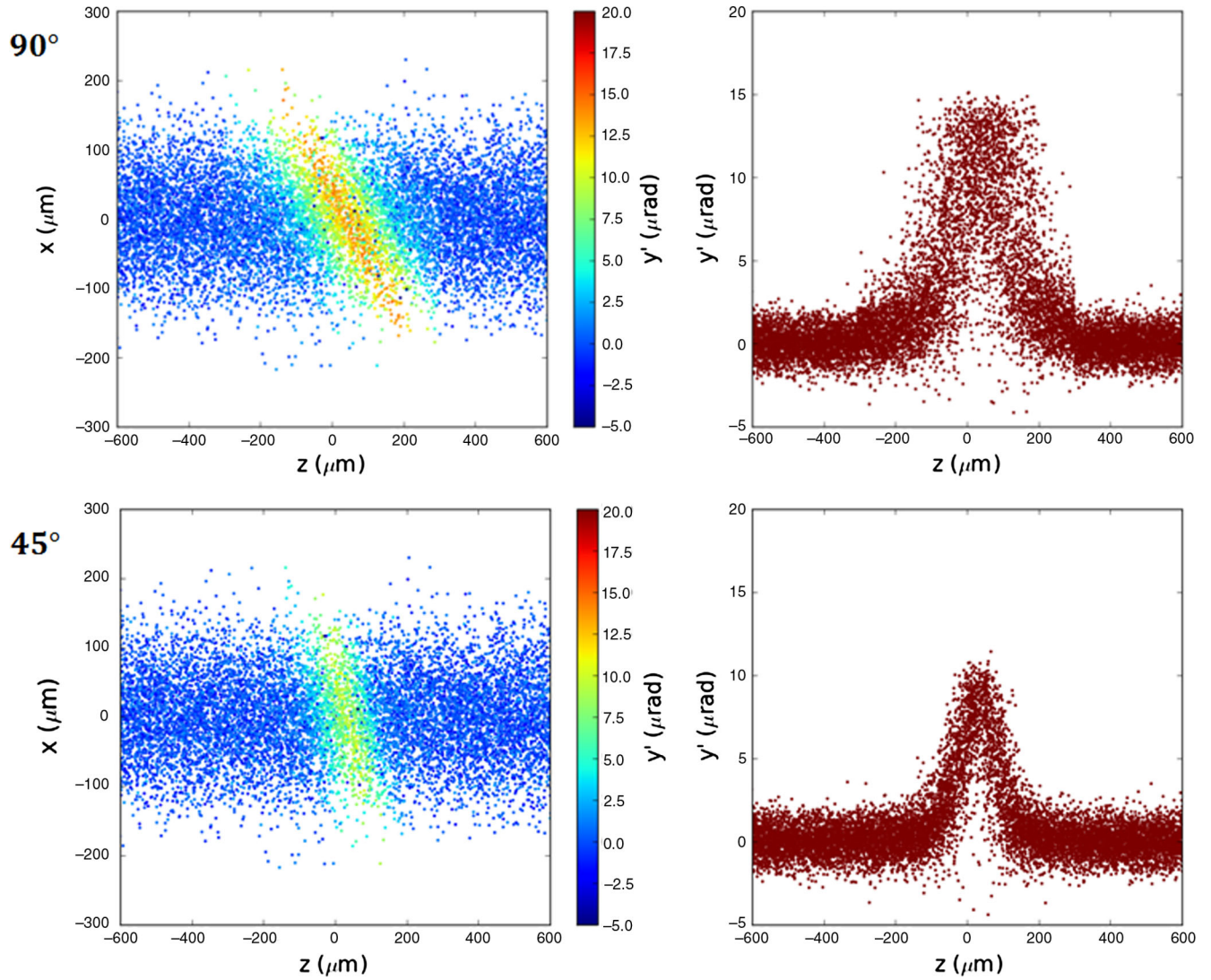


FIG. 13. Compare phase space distribution in the  $(z, x)$  plane and the  $(z, y')$  plane for  $90^\circ$  and  $45^\circ$  respectively.

## V. SPECIFIC EXAMPLE

### A. Slice profile at kicker and radiator

We use the 6D phase space distribution shown in Fig. 6 for the low energy bunch from the linac compressor simulation with 22 MeV, 200 pC as an example to calculate the slice profile. The formula for angular kick gives the optimum vertical distance from the linac beam to the storage ring beam as  $35 \mu\text{m}$ . Since the maximum angular kick is determined by these parameters already, to improve angular separation of the slice from the core, we should choose the crossing point in the storage ring with maximum  $\beta_y$  to minimize the core vertical divergence. In the meantime, since the longer crossing time increases the slice pulse length, we need to minimize  $\beta_x$  so that the horizontal beam size is small. This criterion leads us to choose the slicing point at the position of either about 8.3 m (point A) or 19.3 m (point B) in Fig. 8 where  $\beta_x = 3.8 \text{ m}$ ,  $\beta_y = 25 \text{ m}$ . These two positions are both located next to the dipoles.

They have vertical betatron phase advances from the radiator U20 at position 26 m of about  $125^\circ$  and  $88^\circ$  respectively. Using the 6D distribution of the linac bunch at the final focus point shown in Fig. 6, we calculate the angular kick received by particles in the storage ring bunch after the crossing and plot the phase space distribution. In Fig. 9 we show the phase space for  $y'$  versus  $z$  right after the kick with crossing  $z$  at 8.3 m. In this plot we use the color scale as  $z$ , to give an impression of the short pulse length. In Fig. 10, we show  $y'$  versus  $y$  at the crossing point at 8.3 m, right after the kick.

TABLE II. Quantitative comparison of  $90^\circ$  and  $45^\circ$  crossing angle.

	$\sigma_t$ [fs]	$\sigma_{y,\text{slice}}/\sigma_{y,\text{core}}$ [ $\mu\text{m}/\mu\text{m}$ ]	Slice fraction [%]	$\varepsilon_{y,\text{slice}}/\varepsilon_{y,\text{core}}$ [pm/pm]	$\Delta y/\sigma_{y,\text{core}}$ [pm/pm]
$90^\circ$	320	12.5/3.3	2	43.7/10	38/3.3
$45^\circ$	150	7.03/3.3	1	22/10	29/3.3

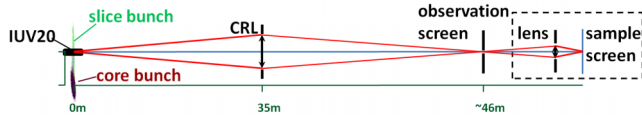


FIG. 14. Conceptual optical scheme of electron beam slicing beam line at NSLS-II.

Figure 11 gives the phase space plot of  $y$  versus  $y'$  at the radiator at 26 m. We compared the results using the 6D simulated bunch with the results using a Gaussian distribution of the same rms beam size as the simulated linac bunch. They are very close and hardly distinguishable visibly. This indicates the Gaussian assumption of the bunch's 3D distribution in Sec. II A is an excellent approximation and this makes it easy to use the rms

beam size of the linac bunch to estimate the kick effects quickly.

Figure 9 shows a thin slice is kicked up right after the crossing, while Fig. 10 shows how the slice is separated from the core in  $(y, y')$  phase space, right after the kick. Figure 11 shows the same phase space after a  $125^\circ$  phase advance at the radiator. The transport of phase space distribution is carried out by the tracking code ELEGANT [22]. The phase space rotation is such that the slice can be separated from the core both angularly and spatially. To understand the separation from the core, we draw a vertical line at about  $15 \mu\text{m}$  from the core indicating the  $5\sigma$  separation boundary and calculate the properties of the slice. We find in this case the center of the slice is  $38 \mu\text{m}$  from the core, while the rms size of the core is  $3.3 \mu\text{m}$ . Thus the spatial separation is more than 10

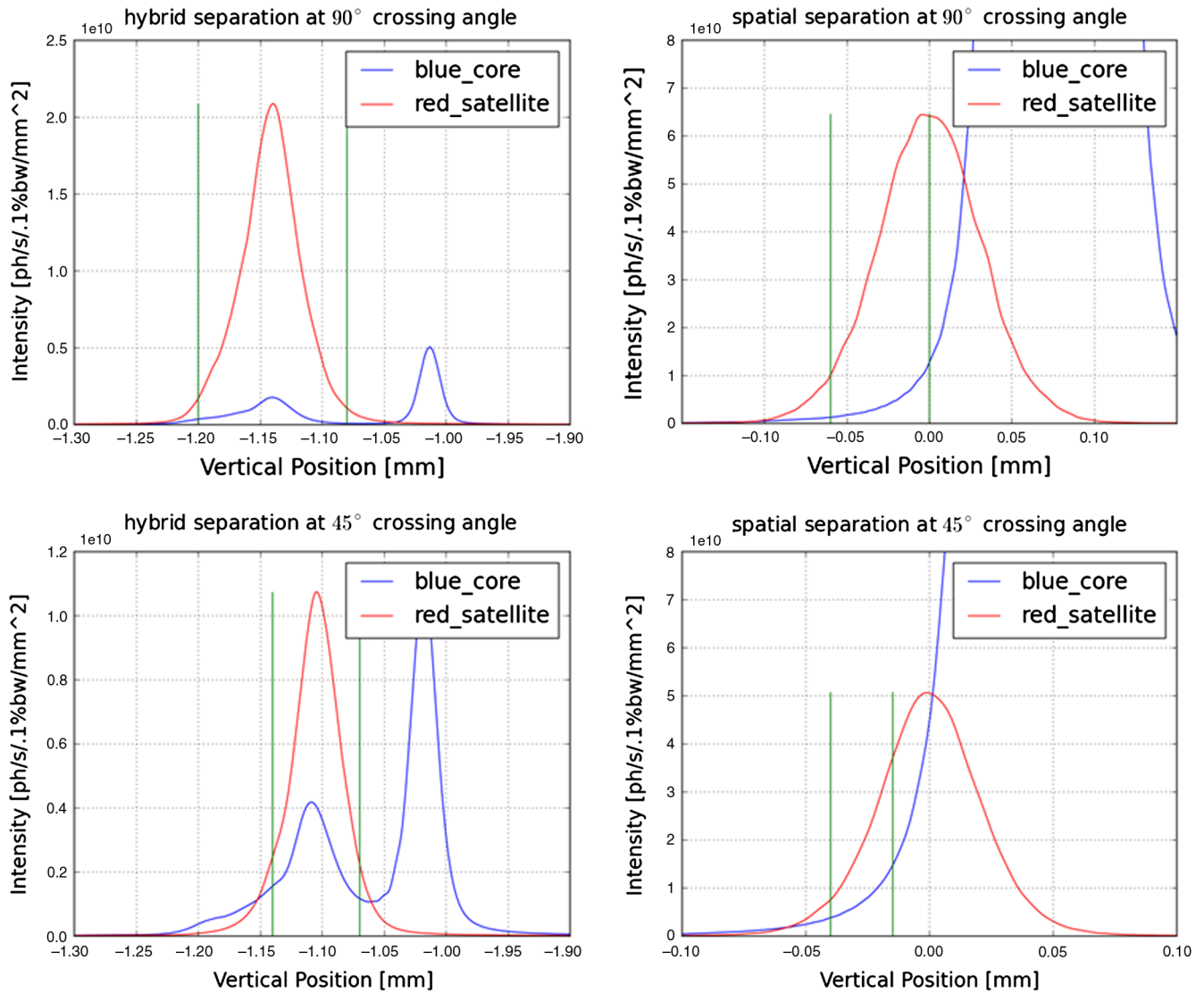


FIG. 15. Vertical cuts of the intensity distribution at the observation plane of the core (blue curve) and the satellite (red curve) using different separation methods for  $90^\circ$  and  $45^\circ$  respectively. The green lines represent the apertures used to block the main part of the core radiation for noise reduction. The power calculated is proportional to the area between the green lines. Upper-left figure: hybrid separation at  $90^\circ$ . Upper-right figure: spatial separation at  $90^\circ$ . Lower-left figure: hybrid separation at  $45^\circ$ . Lower-right figure: spatial separation at  $45^\circ$ .

times the core size. In addition there is a mixture of angular separation of about  $25 \mu\text{rad}$  to improve the separation. We find the fraction of the slice separated is 2% in this case. The slice size is  $12.5 \mu\text{m}$ , larger than the core size of  $3.3 \mu\text{m}$ . The vertical emittance of the slice increases from  $9.5 \text{ pm}$  of the core to  $43.7 \text{ pm}$ .

The rms slice length in this case is  $320 \text{ fs}$ , much larger than the linac bunch length of  $128 \text{ fs}$ . This is because the horizontal crossing time at the interaction point at  $8.3 \text{ m}$  in Fig. 8. Since  $\beta_x = 3.8 \text{ m}$  at this point, for horizontal emittance of  $1 \text{ nm}$ , the rms beam size here is  $61 \mu\text{m}$  corresponding to about  $200 \text{ fs}$  crossing time. It is possible to reduce the pulse length due to the crossing time by reducing the crossing angle, for example from  $90^\circ$  to  $45^\circ$  between the forward direction of the linac beam and the storage ring beam. This is illustrated in Fig. 12 showing at  $45^\circ$  the linac bunch has a velocity component parallel to the storage ring bunch making the slice shorter. The simulation shows the bunch length is reduced to  $150 \text{ fs}$  at the expense of only a small reduction of spatial separation from  $38 \mu\text{m}$  to  $29 \mu\text{m}$ . In Fig. 13 we compare the phase space distribution for the  $90^\circ$  crossing and  $45^\circ$  crossing. The left plot is for the  $(z, x)$  phase space with the color scale representing the kick angle, clearly showing the tilted distribution for the case of  $90^\circ$  gives longer pulse length in the  $z$  direction. In the right of the plot we give the distribution in  $(z, y')$  plane, showing clearly the reduction of pulse length for  $45^\circ$  crossing. Table II gives the comparison of quantitative analysis of these two cases. The rms pulse length of the slice is reduced from  $320$  to  $150 \text{ fs}$  when the crossing angle is  $45^\circ$ . The data also give other details about the slice generated. A more detailed description of angled crossing will be given in a separate paper [14].

### B. Radiation separation

The thin slice bunch and core bunch pass through the  $3 \text{ m}$  long U20 in-vacuum undulator and radiate x-ray pulses of length  $150\text{--}320 \text{ fs}$  (depending on the crossing angle) and  $30 \text{ ps}$  respectively. Due to the spatial and angular differences in vertical phase space of the two bunches, the very short, satellite hard x-ray radiation can

be separated from the core bunch radiation with sufficient signal to noise ratio (SNR). We propose a conceptual optical scheme [23] shown in Fig. 14 allowing for the separation of the satellite radiation from the core and the transport of the short x-ray pulse to a sample. The scheme includes a prefocusing compound refractive lens or a mirror, a secondary source aperture and a final focusing mirror. To get reliable estimates of the separation performances, a wavefront propagation study was performed using the Synchrotron Radiation Workshop (SRW) physical optics computer code [24].

Two methods are used to separate the radiations. One is the pure spatial separation, and the other one is the spatial and angular hybrid separation. The vertical cuts of the intensity distribution on the observation screen are illustrated in Fig. 15 showing the separation of the core radiation (the blue curve) and the satellite radiation (the red curve) using different separate methods with crossing angle  $90^\circ$ ,  $45^\circ$  respectively. The separate performances on the observation screen are shown in Table III. For example, at  $90^\circ$  crossing angle, using spatial and angular hybrid separation, the separate SNR is 12 and the flux per pulse reaches  $10000 \text{ photons}/0.1\% \text{ BW}$  at the expense of relatively longer  $320 \text{ fs}$  pulse length. Since the repetition rate can reach  $100 \text{ kHz}$  as described in Sec. IV, the average flux per second for this case can reach  $1 \times 10^9 \text{ photons}/\text{sec}/0.1\% \text{ BW}$ . At  $45^\circ$  crossing angle, the satellite hard x-ray pulse  $150 \text{ fs}$  is much shorter. The smaller angular kick results in a smaller SNR at 2.7. However, this SNR is calculated based on an assumption that without considering the time resolution of the detector, x-ray from all the core electrons contributes to the noise. If a fast detector with a time resolution around several picoseconds [2,25–27] is used in the femtosecond x-ray diffraction experiment, the SNR can increase significantly. For example, if the detector's time resolution is  $10 \text{ ps}$ , then the SNR is increased to 8 at  $45^\circ$  crossing angle as shown in Table III. The data in Table III indicate the SNR is around 5–12 and the average satellite photon flux per second reaches  $5 \times 10^8\text{--}2 \times 10^9 \text{ photons}/\text{sec}/0.1\% \text{ BW}$  depending on the separation methods and the crossing angle between the slice bunch and the core bunch.

TABLE III. Separation performances of hard x-ray synchrotron radiation from electron beam slices. Data are recorded at  $7.8 \text{ KeV}$  on the observation screen.

Crossing angle	Separate type	Flux/pulse <sup>a</sup>	Flux <sup>b</sup>	Peak intensity	Pulse length	
		[photons/0.1%bw]	[photons/ sec /0.1%bw]	[photons/ sec /0.1%bw/mm <sup>2</sup> ]	SNR	[fs]
$90^\circ$	Spatial + angular	$10 \times 10^3$	$10 \times 10^8$	$2.1 \times 10^{10}$	12	320
	Spatial	$18 \times 10^3$	$18 \times 10^8$	$6.5 \times 10^{10}$	5	320
$45^\circ$	Spatial + angular	$5 \times 10^3$	$5 \times 10^8$	$1.1 \times 10^{10}$	8 <sup>c</sup> (2.6)	150
	Spatial	$5 \times 10^3$	$5 \times 10^8$	$3.6 \times 10^{10}$	8 <sup>c</sup> (2.7)	150

<sup>a</sup>Assume NSLS-II's revolution time is about  $2.6 \mu\text{s}$ , then flux/pulse = power  $\times 2.6 \mu\text{s}$ .

<sup>b</sup>Assume the repetition rate of the low energy linac is  $100 \text{ kHz}$ , then flux = flux/pulse  $\times 100 \text{ kHz}$ .

<sup>c</sup>With  $10 \text{ ps}$  of the detector's time resolution.

## VI. CONCLUSION AND DISCUSSION

In conclusion, our simulation of the low energy compressor, the analysis of the phase space distribution of the slice and the separation of the satellite x-ray radiation from the core radiation have clearly confirmed the feasibility of electron beam slicing approach as a new method of the generation of short x-ray pulses. There is a trade off between the cost and the x-ray pulse performances: increasing the linac bunch's energy and charge can increase the kick angle and improve the hard x-ray performances. Depending on the user's detailed requirements, we can adjust the linac bunch's energy and charge to meet the final required x-ray pulse length and flux. There is also a trade off between the crossing angle and the pulse length and signal noise ratio: reducing the crossing angle from 90° to 45° can significantly reduce the pulse length at the expense of the signal noise ratio.

In future experiments, a possible issue will be the time jitter between the low energy bunches and the lasers used in a pump-probe experiment. For example, in Ref. [21] we find it is possible to use a laser-optical synchronization system to realize the time-resolved measurements with femtosecond precision. Another possible issue is the use of the low energy linac beam for the generation of THz signal in the pump-probe experiments.

## ACKNOWLEDGMENTS

We appreciate Dr. John Corlett and Dr. Ji Qiang for providing detailed data on the APEX rf gun, and guidance on the application of IMPACT-T. We appreciate Dr. Oleg Chubar for guidance on the use of SRW and the separation calculation of the core-slice radiation. We wish to acknowledge the support of our colleagues: Timur Shaftan, Raymond Filler, Yongjun Li, Lingyun Yang, Guimei Wang, Yoshiteru Hidaka, Weiming Guo, James Rose, and Sam Krinsky in offering much help and suggestions. This work was funded by DOE under Contracts No. LDRD12-023 and No. LDRD14-022.

## APPENDIX A: PROFILE FUNCTION WHEN $\rho \gg 1$

When  $\rho \gg 1$ , the profile function Eq. (6) becomes

$$\begin{aligned} f_y(\rho \gg 1, \bar{u}_1 = 0, \bar{y}_1 = 1) & \\ &= \int_0^\infty \text{Re}[W(iy)] [e^{-(\rho y - \bar{y}_1)^2} - e^{-(\rho y + \bar{y}_1)^2}] dy \\ &= \frac{1}{\rho} \int_0^\infty \text{Re} \left[ W \left( i \frac{y}{\rho} \right) \right] [e^{-(y - \bar{y}_1)^2} - e^{-(y + \bar{y}_1)^2}] dy. \quad (\text{A1}) \end{aligned}$$

Due to  $\bar{y}_1 = 1$ , the contribution of the factor  $[e^{-(y - \bar{y}_1)^2} - e^{-(y + \bar{y}_1)^2}]$  to the profile function  $f_y$  comes from  $y \sim 1$ , then we have  $y/\rho \ll 1$ . This leads to  $W(i \frac{y}{\rho}) = 1$ . Then we have

$$\begin{aligned} f_y(\rho \gg 1, \bar{u}_1 = 0, \bar{y}_1 = 1) & \\ &\approx \frac{1}{\rho} \int_0^\infty [e^{-(y - \bar{y}_1)^2} - e^{-(y + \bar{y}_1)^2}] dy \\ &= \frac{\sqrt{\pi}}{\rho} \text{erf}(1), \quad (\text{A2}) \end{aligned}$$

where  $\text{erf}(z) = \frac{2}{\sqrt{\pi}} \int_0^z e^{-t^2} dt$ .

## APPENDIX B: EMITTANCE INCREASE

The emittance of individual particle is defined as

$$J_j = \frac{1}{2} (\gamma y_j^2 + 2\alpha y_j y_j' + \beta y_j'^2) = \frac{1}{2\beta} [y_j^2 + (\alpha y_j + \beta y_j')^2] \quad (\text{B1})$$

and the beam emittance is

$$\varepsilon = \sqrt{\langle y_j^2 \rangle \langle y_j'^2 \rangle - \langle y_j y_j' \rangle^2} = \langle J_j \rangle. \quad (\text{B2})$$

Assume the particle's emittance before and after kick are respectively

$$J_j = \frac{1}{2\beta} [y_j^2 + (\alpha y_j + \beta y_j')^2] \quad (\text{B3})$$

and

$$J_{1j} = \frac{1}{2\beta} [y_j^2 + (\alpha y_j + \beta y_{1j}')^2], \quad (\text{B4})$$

then the emittance increase for the individual particle can be written as

$$\delta J_j = \frac{1}{2\beta} [2\alpha\beta y_j \delta y_j' + \beta^2 (y_{1j}'^2 - y_j'^2)]. \quad (\text{B5})$$

The emittance increase of the whole bunch is

$$\delta \varepsilon = \langle \delta J_j \rangle = \frac{\beta}{2} \langle y_{1j}'^2 - y_j'^2 \rangle = \frac{\beta}{2} (k^2 - 1) \langle y_j'^2 \rangle, \quad (\text{B6})$$

where we use  $\langle y_j \delta y_j' \rangle = 0$  and assume  $y_{1j}' = ky_j'$ .

- 
- [1] A. Zholents and M. Zolotarev, *Phys. Rev. Lett.* **76**, 912 (1996).
  - [2] R. W. Schoenlain, S. Chattopadhyay, H. H. W. Chong, T. E. Glover, P. A. Heimann, C. V. Shank, A. A. Zholents, and M. S. Zolotarev, *Science* **287**, 2237 (2000).
  - [3] S. Khan and H. A. Durr, in *Proceedings of the 8th European Particle Accelerator Conference, Paris, 2002* (EPS-IGA and CERN, Geneva, 2002).
  - [4] G. Ingold, A. Streun, B. Singh, R. Abela, P. Beaud, G. Knopp, L. Rivkin, V. Schlott, Th. Schmidt *et al.*, in

- Proceedings of the 19th Particle Accelerator Conference, Chicago, Illinois, 2001* (IEEE, Piscataway, NJ, 2001).
- [5] C. Steier *et al.*, in *Proceedings of the 2003 Particle Accelerator Conference, Portland, OR* (IEEE, New York, 2003).
- [6] O. Chubar and P. Elleaume, in *Proceedings of the 6th European Particle Accelerator Conference, Stockholm, 1998* (IOP, London, 1998).
- [7] A. Zholents, P. Heimann, M. Zolotarev, and J. Byrd, *Nucl. Instrum. Methods Phys. Res., Sect. A* **425**, 385 (1999).
- [8] M. Katoh, *Jpn. J. Appl. Phys.* **38**, L547 (1999).
- [9] M. Borland, *Phys. Rev. ST Accel. Beams* **8**, 074001 (2005).
- [10] P. Emma, in *Proceedings of the 23rd Particle Accelerator Conference, Vancouver, Canada, 2009* (IEEE, Piscataway, NJ, 2009).
- [11] J. N. Galayda, The Linac Coherent Light Source Project No. SLAC-PUB-10115, 2002.
- [12] F. Willeke and L. H. Yu, in *Proceedings of International Particles Accelerator Conference 2013, Shanghai, China*.
- [13] L. D. Landau and E. M. Lifshitz, *The Classical Theory of Fields* (Addison-Wesley Press, Cambridge, 1951).
- [14] A. He, F. Willeke, and L. H. Yu (unpublished).
- [15] *NLS-II Source Properties and Floor Layout (2010)*.
- [16] F. Sannibale, B. Bailey, K. Baptiste, J. Byrd, C. Cork, J. Corlett *et al.*, in *Proceedings of International Particles Accelerator Conference 2012, New Orleans, Louisiana, USA*.
- [17] J. Qiang, Report No. LBNL-62326, 2007.
- [18] A. He, Y. Hidaka, T. Shaftan, G. Wang, F. Willeke, L. Yang, and L. H. Yu, in *Proceedings of International Particles Accelerator Conference 2013, Shanghai, China*.
- [19] M. Ehrgott, *Multicriteria Optimization* (Springer, New York, 2005).
- [20] A. He, J. Qiang, L. Yang, L. H. Yu, and F. Willeke (unpublished).
- [21] F. Lohl, V. Arsov, M. Felber, K. Hacker, W. Jalmuzna, B. Lorbeer, F. Ludwig, K.-H. Matthiesen, H. Schlarb, B. Schmidt, P. Schmuser, S. Schulz, J. Szewinski, A. Winter, and J. Zemella, *Phys. Rev. Lett.* **104**, 144801 (2010).
- [22] M. Borland, ANL Advanced Photon Source Report No. LS-287, 2000.
- [23] A. He, O. Chubar, and L. H. Yu (unpublished).
- [24] O. Chubar, P. Elleaume, S. Kuznetsov, and A. Snigirev, in *Proc. SPIE Int. Soc. Opt. Eng.* **4769**, 145 (2002).
- [25] A. Rousse, C. Rischel, and J. C. Gauthier, *Rev. Mod. Phys.* **73**, 17 (2001).
- [26] A. M. Lindenberg, I. Kang, S. L. Johnson, T. Missalla, P. A. Heimann, Z. Chang, J. Larsson, P. H. Bucksbaum, H. C. Kapteyn, H. A. Padmore, R. W. Lee, J. S. Wark, and R. W. Falcone, *Phys. Rev. Lett.* **84**, 111 (2000).
- [27] Z. Chang, A. Rundquist, J. Zhou, M. M. Murnane, H. C. Kapteyn, X. Liu, B. Shan, J. Liu, M. Gong, and X. Zhang, *Appl. Phys. Lett.* **69**, 133 (1996).